Tran-SET

Transportation Consortium of South-Central States

Solving Emerging Transportation Resiliency, Sustainability, and Economic Challenges through the Use of Innovative Materials and Construction Methods: From Research to Implementation

Optimizing the Geometric Configuration and Manufacturing Process of High Mast Illumination Poles

Project No. 19STUTSA02

Lead University: University of Texas at San Antonio

Final Report

August 2020

Disclaimer

The contents of this report reflect the views of the authors, who are responsible for the facts and the accuracy of the information presented herein. This document is disseminated in the interest of information exchange. The report is funded, partially or entirely, by a grant from the U.S. Department of Transportation's University Transportation Centers Program. However, the U.S. Government assumes no liability for the contents or use thereof.

TECHNICAL DOCUMENTATION PAGE

1. Project No.	2. Government Accession No.	3. Recipient's Catalog No.
19STUTSA02		

4. Title and Subtitle	5. Report Date
Optimizing the Geometric Configuration and Manufacturing Process of High Mast Illumination Poles	Aug. 2020
	6. Performing Organization Code
7. Author(s)	**8. Performing Organization Report No.**
PI: Arturo Montoya https://orcid.org/ 0000-0003-1429-5105 Co-PI: Adolfo Matamoros https://orcid.org/0000-0002-5312-7764 GRA: Reza Nasouri https://orcid.org/0000-0001-7232-9372 GRA: Echizeni Ikpah https://orcid.org/0000-0001-7072-4918 GRA: Arsalan Majlesi https://orcid.org/0000-0001-5514-1562	
9. Performing Organization Name and Address	**10. Work Unit No. (TRAIS)**
Transportation Consortium of South-Central States (Tran-SET) University Transportation Center for Region 6 3319 Patrick F. Taylor Hall, Louisiana State University, Baton Rouge, LA 70803	**11. Contract or Grant No.** 69A3551747106
12. Sponsoring Agency Name and Address	**13. Type of Report and Period Covered**
United States of America Department of Transportation Research and Innovative Technology Administration	Final Research Report Aug. 2019 – Aug. 2020
	14. Sponsoring Agency Code

15. Supplementary Notes

Report uploaded and accessible at Tran-SET's website (http://transet.lsu.edu/).

16. Abstract

This work presents the development of a high-fidelity model that accounts for the cumulative effect of welding and hot-dip galvanizing on the determining the resulting residual stresses and deformations induced during the manufacturing process of high mast illumination poles (HMIPs). This model is meant to elucidate the root causes of weld toe cracks in HMIPs. A TxDOT pole-to-base plate connection detail was used as the reference model in the analysis. Welding was modeled using the plug-in Abaqus Welding Interface (AWI), which automatically implements a series of sequential thermal and mechanical analyses. Then, the welding stress results were used as initial input to the galvanizing analysis. The cumulative stress results were compared against simulations that only considered the galvanizing process. A parametric study was then conducted to quantify the variation in the residual stresses and equivalent plastic strain magnitudes induced during the welding and galvanizing of HMIPs due to changes in welding and galvanizing practices. The results revealed that the cumulative effects of the different processes involved in the manufacturing of HMIPs contribute to the formation of galvanizing cracks in HMIPs. Also, increasing the dipping submersion speed during galvanizing and lowering the torch temperature magnitude during welding results in fewer zones prone to cracking. Altering the angle of inclination effect did not have a significant impact on the results. Performing variations in the manufacturing practices used for the fabrication of HMIPs can contribute to reducing the extensive inspection procedures conducted post-galvanizing to identify cracks.

17. Key Words	18. Distribution Statement
High Mast Illumination Poles, Welding, Galvanizing, Residual Stresses, Plastic Deformation	No restrictions. This document is available through the National Technical Information Service, Springfield, VA 22161.

19. Security Classif. (of this report)	20. Security Classif. (of this page)	21. No. of Pages	22. Price
Unclassified	Unclassified	29	

Form DOT F 1700.7 (8-72) **Reproduction of completed page authorized.**

SI* (MODERN METRIC) CONVERSION FACTORS

APPROXIMATE CONVERSIONS TO SI UNITS

Symbol	When You Know	Multiply By	To Find	Symbol
		LENGTH		
in	inches	25.4	millimeters	mm
ft	feet	0.305	meters	m
yd	yards	0.914	meters	m
mi	miles	1.61	kilometers	km
		AREA		
in^2	square inches	645.2	square millimeters	mm^2
ft^2	square feet	0.093	square meters	m^2
yd^2	square yard	0.836	square meters	m^2
ac	acres	0.405	hectares	ha
mi^2	square miles	2.59	square kilometers	km^2
		VOLUME		
fl oz	fluid ounces	29.57	milliliters	mL
gal	gallons	3.785	liters	L
ft^3	cubic feet	0.028	cubic meters	m^3
yd^3	cubic yards	0.765	cubic meters	m^3
		NOTE: volumes greater than 1000 L shall be shown in m^3		
		MASS		
oz	ounces	28.35	grams	g
lb	pounds	0.454	kilograms	kg
T	short tons (2000 lb)	0.907	megagrams (or "metric ton")	Mg (or "t")
		TEMPERATURE (exact degrees)		
^oF	Fahrenheit	5 (F-32)/9 or (F-32)/1.8	Celsius	^oC
		ILLUMINATION		
fc	foot-candles	10.76	lux	lx
fl	foot-Lamberts	3.426	$candela/m^2$	cd/m^2
		FORCE and PRESSURE or STRESS		
lbf	poundforce	4.45	newtons	N
lbf/in^2	poundforce per square inch	6.89	kilopascals	kPa

APPROXIMATE CONVERSIONS FROM SI UNITS

Symbol	When You Know	Multiply By	To Find	Symbol
		LENGTH		
mm	millimeters	0.039	inches	in
m	meters	3.28	feet	ft
m	meters	1.09	yards	yd
km	kilometers	0.621	miles	mi
		AREA		
mm^2	square millimeters	0.0016	square inches	in^2
m^2	square meters	10.764	square feet	ft^2
m^2	square meters	1.195	square yards	yd^2
ha	hectares	2.47	acres	ac
km^2	square kilometers	0.386	square miles	mi^2
		VOLUME		
mL	milliliters	0.034	fluid ounces	fl oz
L	liters	0.264	gallons	gal
m^3	cubic meters	35.314	cubic feet	ft^3
m^3	cubic meters	1.307	cubic yards	yd^3
		MASS		
g	grams	0.035	ounces	oz
kg	kilograms	2.202	pounds	lb
Mg (or "t")	megagrams (or "metric ton")	1.103	short tons (2000 lb)	T
		TEMPERATURE (exact degrees)		
^oC	Celsius	1.8C+32	Fahrenheit	^oF
		ILLUMINATION		
lx	lux	0.0929	foot-candles	fc
cd/m^2	$candela/m^2$	0.2919	foot-Lamberts	fl
		FORCE and PRESSURE or STRESS		
N	newtons	0.225	poundforce	lbf
kPa	kilopascals	0.145	poundforce per square inch	lbf/in^2

TABLE OF CONTENTS

LIST OF FIGURES

LIST OF TABLES

ACRONYMS, ABBREVIATIONS, AND SYMBOLS

AASHTO	American Association of State Highway and Transportation Officials
ASTM	American Society for Testing and Materials
AWI	Abaqus Welding Interface
FEM	Finite Element Method
HMIP	High Mast Illumination Poles
PEEQ	Equivalent Plastic Strain
TxDOT	Texas Department of Transportation

EXECUTIVE SUMMARY

Galvanization is a widely used, effective method to protect steel from corrosion. However, in the past two decades, post-galvanizing inspections have reported the presence of cracks in high mast illumination poles (HMIPs), particularly at the toe of the welded connection between the pole and the base plate, on the pole. These flaws impose a risk to the public as they can propagate during service due to cyclic wind loads. Nonetheless, as each of the fabricating stages, i.e., cold working, welding, and hot-dip galvanizing, induce residual stresses in the steel, the crack formation phenomenon cannot be solely attributed to the galvanizing process. The main goal of this work is to provide guidance to engineers, galvanizers, and fabricators on how to minimize the likelihood of crack initiation during the fabrication process of high mast illumination poles (HMIPs).

Most research efforts up to date have concentrated on understanding the factors that contribute to the propagation of galvanization flaws once the HMIP is under service. The effects of pole shape on fatigue performance of high-mast lighting towers subject to wind loads have been investigated through experimental tests. Researchers have also made efforts to track the mechanical behavior of HMIPS during their galvanizing process. However, the high temperatures of the hot zinc bath limit the stress, strain, and deformation measurements that can be recorded during galvanizing; hence, experimental studies have been complemented with numerical simulations to quantify the response of HMIPs during galvanization, as well as the stress demands when the poles are in service and subject to wind-induced fatigue loads.

This research work focused on developing a better understanding of the root causes of weld toe crack in HMIPs by capturing the cumulative effects of both the welding and the galvanizing fabrication processes in HMIPs. This research objective was achieved by conducting three-dimensional finite element analyses on an HMIP with a Texas Department of Transportation (TxDOT) pole-to-base plate connection detail. For modeling the welding of HMIPs, the plug-in Abaqus Welding Interface (AWI) was used. The AWI tool facilitates the welding process by automatically implementing a series of sequential thermal and mechanical analyses. The parameters of both welding (torch temperature) and galvanizing (submersion speed and angle of inclination) were varied to determine their influence on the crack formation phenomenon occurring post galvanizing.

The results revealed that the cumulative effects of the different processes involved in the manufacturing of HMIPs contribute to the formation of galvanizing cracks in HMIPs. Also, increasing the dipping submersion speed during galvanizing and lowering the torch temperature magnitude during welding results in fewer zones prone to cracking. Altering the angle of inclination effect did not have a significant impact on the results. Performing variations in the manufacturing practices used to fabricate HMIPs can minimize the extensive inspection procedures conducted post-galvanizing to identify cracks.

1. INTRODUCTION

High Mast Illumination Poles (HMIPs) are tall steel poles that support lighting attached to the top to illuminate areas such as highways, airports, and parking lots. They play a crucial role in the economy by extending operations to the nighttime. Since HMIPs are mostly exposed to the environment, they are prone to corrosion. Galvanization is an effective method used industrially since the 1800s to remedy against corrosion.

In the past two decades, several state transportation agencies have reported numerous fatigue failures of HMIPs. These failure cases led to post galvanizing inspection and research that identified the region of crack to be at the toe of the welded connection between the pole and the base plate *(1)–(5)*. The welding and galvanizing process have been identified to produce thermal shock in steel structures with the presence of residual stresses that propagate to cracks *(5, 6)*. Experimental and 3D simulation done by Kleineck *(7)* set the rudimentary that the initiation of crack in HMIPs is the galvanizing process. Further studies *(8)* used more sophisticated 3D finite element models to predict the residual stresses and plastic strains generated during galvanizing. However, there is little information on the literature regarding the influence of the welding procedure on forming the weld toe cracks in HMIPs.

In this study, the cumulative effect of the welding and galvanization of HMIPs is investigated using commercial software ABAQUS to create a 3D Finite Element (FE) model of temperature-dependent material properties. The welding simulation precedes the coupled galvanization simulation with an uncoupled thermomechanical model created through the ABAQUS Welding Interface (AWI) plugin.

2. OBJECTIVES

This research work focuses on developing a better understanding of the root causes of weld toe crack in HMIPs by capturing the cumulative effects of both welding and galvanizing. This research objective was achieved by developing a three-dimensional finite element analysis capable of simulating the welding and galvanizing of HMIP and performing a parametric study in which the parameters of both welding and galvanizing were varied to determine their influence on the crack formation phenomenon occurring post galvanizing. These variables' effects on the likelihood of cracks developing during galvanizing were quantified by comparing the resulting residual stresses and equivalent plastic strains magnitudes generated during the simulations.

3. LITERATURE REVIEW

The fabrication of High-mast Illumination Poles (HMIPs) involves a series of stages, including cold working, welding, and hot-dip galvanizing. The poles are made from steel sheets. Typically, the steel arrives at the factory as a large roll. Fabricators use a decoiler to roll out the sheet and make it flat. The pole's desired shape is achieved through cold-working operations, which consists of bending the steel sheets into a polygonal shape using a press brake or rolling the sheet into a circular shape of the desired diameter. The edges of the sheet are joined by seam welding. Then, the bottommost section is welded to an annular base plate. It should be noted that HMIP pole geometry and pole-to-base plate standard connection details vary by state.

The exposure of HMIPs to the environment during their service life subjects them to corrosion damage. These structures are protected from corrosion through hot-dip galvanization. This is an economical and effective method of preventing steel components from corrosion by submerging them in a molten hot zinc bath (with temperature varying from 445 to 455°C). The zinc reacts on the steel surface to form an intermetallic coating layer that protects the metal from the corrosive environment *(9-13)*.

In recent years, post-galvanizing inspections have reported the presence of cracks in HMIPs, particularly at the toe of the welded connection between the pole and the base plate, on the pole *(2), (4), (7), (13)–(15)*. These cracks have been identified at the welded toe of the pole to base connection. Dawood et al. *(6)* identified a complex interaction between the manufacturing processes of HMIPs, i.e., cold working, welding, and galvanizing, as the likely cause of the crack. Nonetheless, the root cause of crack formation is yet to be understood. According to *(16)*, recent changes in the zinc bath composition of the galvanization techniques may also be contributing to crack formation. Kinstler *(16)* also suggested that the cracks may have existed before the galvanization and they have come detected in recent years as a result of improved inspection techniques and dissemination of data.

Several studies *(17)–(19)* have investigated the fatigue life of damaged poles due to wind excitations. As fatigue failure originates from localized cracks, the evaluation of structural durability and welded joints failure is measured by using a local approach that includes material characteristics in the vicinity of cracks, effects of geometry and loading *(17)*. The most widely used approaches include hot spot structural stress methods for estimating fatigue strength *(20)*, notch stress/strain analyses for determining crack initiation, and fracture mechanics. However, these studies have omitted to identify the cause of cracks.

Research by Dawood *(6)* was amongst the first to consider fatigue on Texas connections. Improvements to the Texas state design by the inclusion of backing-ring to extend the poles' fatigue life were followed *(9, 8, 38-43)*. The Texas detail has been updated to include a backing ring welded over the pole shaft with full penetration weld *(40)* to the base plate. It should be noted that HMIP pole to base plate connection vary from state to state, and so does the geometric configuration and fatigue performance *(13), (14), (21), (22)*.

Due to the difficulty in measuring stress, strain, and deformation fields at the galvanizing plants, experimental studies have been done together with numerical simulations to better understand the response of HMIPs during the galvanization process. The stress demand during the poles' service and when it is subjected to wind-induced fatigue loads is one of the main concerns for researchers in this area. Finite element (FE) analysis was performed by Ocel *(24)* and Warpinski *(23)* on three-

dimensional HMIP models to have a better understanding of the hotspot stresses at the plate connection. The stress concentration factor (SCF) obtained from the simulations was an indicator of the potential of the HMIPs to fatigue concerns. Additionally, Ocel *(24)* performed parametric studies to elucidate the effect of the base plate thickness and the pole's wall thickness on the stress concentration factor. The results showed that the SCF increases slightly with the wall thickness. It was also seen that in a multisided HMIP, the stress concentration factor was enhanced by decreasing the bending angle and that by increasing the thickness of the base plate, the stress concentration factor decreases exponentially. Stam et al. *(14)* also worked on other experimental and numerical cases and concluded that increasing the base plate thickness can undoubtedly be more effective in reducing the stress concentration factor than increasing the shaft thickness. Furthermore, studies performed by Stam et al. *(25)* showed that that the localized strains at pole bends, near the base plate connection, will increase by decreasing the pole thickness. By having a comprehensive look at the result of these studies, we understand that Texas DOT has recommended using thick base plates as a beneficial way to measure the increase in the fatigue life of the HMIPs.

Feldmann *(35)* worked on numerical and experimental models related to steel girders and concluded that dipping with slower speed results in increasing strain parameters and the stress concentration factor. Nguyen *(8,24)* studied the effects of combined welding and galvanizing on steel girders' strain demands. The results showed that the residual strain resulting from the welding significantly affected these girders' susceptibility to cracking. Kleineck *(7)* performed experimental studies to deduce the effect of thermal shocks of HMIPs by attaching strain gauges to measure the deformation of the pole to base plate connection. He also conducted numerical analysis focusing on the mechanical behavior of HMIPs during the galvanizing process. He analyzed an HMIP with a standard pole to base connection and captured the thermally induced strain and stress demands during the galvanizing process. The galvanizing process was modeled using a sequentially-coupled thermal-stress analysis. This study provided a foundation for understanding the effects of galvanizing on HMIPs.

Nasouri et al. *(8,15)* furthered the study by utilizing a finite element model with thermomechanical properties and identified geometric configuration, connections, and regions susceptible to cracking during galvanization. Validation of the FEM model was done by comparing results to experimental studies performed by Kleineck *(7)*. The area around the pole's connection to the base, including welding parts, internal and external collars, was meshed finely to capture the locations that were susceptible to cracking accurately. A coupled temperature displacement analysis was performed using the commercial software Abaqus *(36)* to show interactions between the temperature, strain, displacement, and stress fields during the galvanizing process. The study aimed to evaluate the effects of HMIP geometric configuration on the critical stress and strain demands during galvanizing. The results revealed that the bends were the locations that exhibited the highest demands, which agrees with the typical locations of the weld-toe cracks observed at galvanizing plants. The results also suggested that the dipping stage was critical during the manufacturing process, particularly when the HMIP was partially submerged within the zinc bath. The circular pole model showed stress and strain magnitudes considerably lower than those observed in the multi-sided poles model. The studies by Nasouri et al. *(8,15)* suggested a lack of comparative studies on the behavior of different types of HMIP connections during the galvanization process. The study suggests performing a comprehensive study of the performance of HMIPs with Texas,

Wyoming, and Socket details. Besides, the effects of the welding process on HMIPs were not considered in this study.

Welding precedes the galvanization process and can also contribute to weld-toe crack formation. This method joins the base plate to the pole shaft with heat. A filler material is melted and fuses with the base-metal to join the metallic parts. This process leads to permanent deformation and residual stress in the welded region that may deter the component *(21, 22)*. Remedy for welds defects, post welding treatment *(28), (29),* and inspections add extra cost to the manufacturing process and extend the production time. Due to the reasons above, it is essential to predict the magnitude of residual stresses and the effect of the thermomechanical properties on weld integrity *(30)–(34)*.

Thus, researchers have created, tested and validated numerical methods to simulate welding accurately *(37)–(41)*. The non-uniform relationship between the moving heat source and the thermo-mechanical properties of steel during the welding process makes the predictions of residual stresses exhaustive to storage and computationally expensive, especially in larger structures. The Abaqus Welding Interface (AWI) has served to reduce the computational time compared to the constant Heat Flux Method (CHF) *(29)*. The validation of the model proved accurate with experimental results *(42)*.

4. METHODOLOGY

4.1. Model Description

4.1.1. Model Geometry

The FE model was developed using the commercial finite element software Abaqus *(48)* based on a TxDOT connection detail shown in Figure 1 and dimensions provided in Table 1. The TxDOT connection detail distinguishes from other connection details because it includes a backing ring (or collar) that is placed externally to the pole shaft. The different HMIP parts are attached through welds. A full penetration weld joins the collar and pole shaft to the base plate. The top of the collar is attached to the pole shaft through a fillet weld.

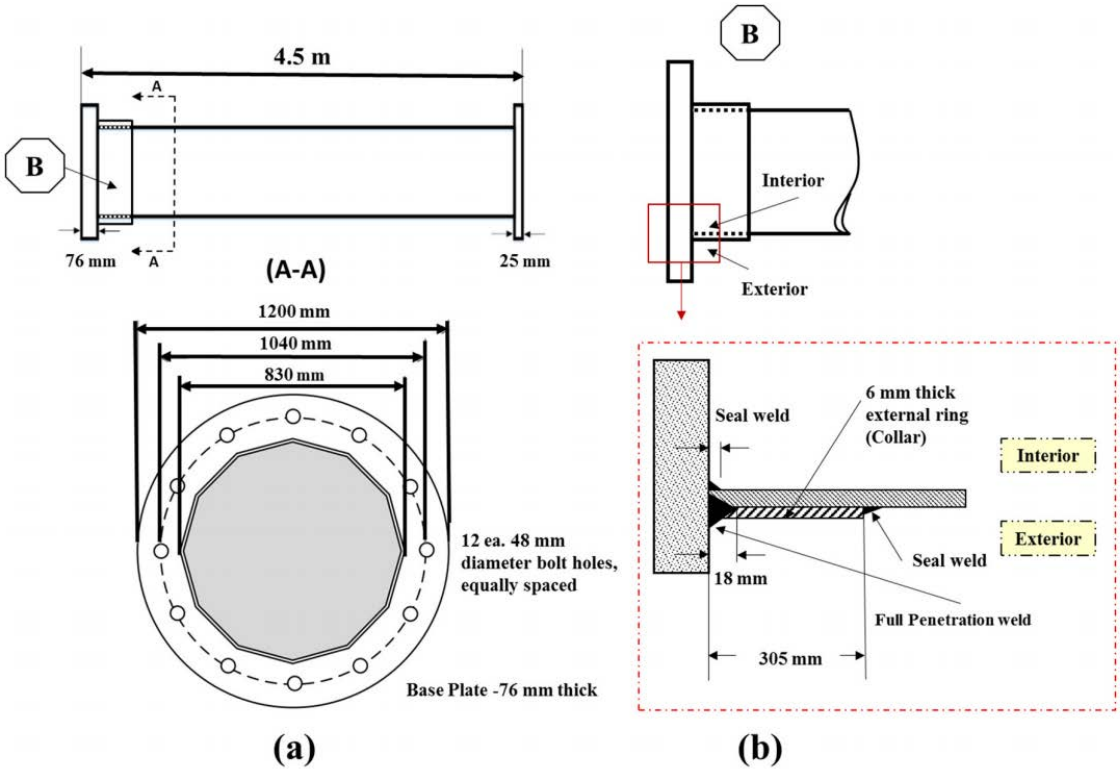

Figure 1. (a) HMIP geometry used in the state of Texas and (b) pole-to-base Plate connection.

Table 1. Geometric properties of the HMIP.

Components	Dimensions (mm)
Base plate diameter	1200
Base plate thickness	76
Access hole diameter	560
Pole shaft diameter	830
Pole shaft thickness	8

Components	Dimensions (mm)
Collar height	305
Collar thickness	6
Top plate thickness	25

The model was simulated using elastic-plastic material properties equivalent to Grade 50 steel (equivalent to ASTM 572-50). The mechanical properties reported by Pilipenko *(43)* and Perić et al. *(44)* were adopted, which are temperature=dependent. The yield stress at room temperature is 345MPa at room temperature. The post-yielding stress-strain response was simulated using isotropic hardening with von Mises yield criterion *(45)*. The thermal and mechanical properties of the base plate steel and weld metal were assumed to be equivalent, following the strategy adopted by several researchers *(18), (44), (46)–(48)* for modeling welded connections. Table 2 provides the parameters used during the analysis.

Table 2. Material Properties of the HMIP.

Young Modulus (GPa)	**Poisson Ratio**	**Density** ($^{kg}/_{mm}$)	**Thermal expansion Coefficient**($^{1}/_{°C}$)	**Specific Heat** ($^{j}/_{mm\,°C}$)	**Thermal Conductivity** ($^{j}/_{mm°C}$)
200	3.35	7.77×10^{-3}	1.2×10^{-5}	3.85×10^{-1}	5.49×10^{-3}

4.1.2 Mesh and Boundary conditions

The model consists of 565,258 nodes and 452,857 eight-nodded linear brick elements. Welding uses a sequential thermal stress analysis procedure; as such, both thermal and mechanical elements, DC3D8 and C3D8 elements in Abaqus were used in the analysis. Coupled thermomechanical elements were used for the galvanizing step of the simulation. The mesh size was kept constant for both the welding and galvanizing procedures. Selecting the appropriate boundary conditions for welding is essential as if the HMIP is overly restrained, this could generate excessively high residual stresses. The boundary conditions were selected based on typical fabrication procedures that simply support the HMIPs at both ends along the vertical direction, y-component. Additional restraints were placed in the x and z directions to prevent the HMIP from overturning within the numerical simulation. The additional restraints were placed at the other end, far away from the welding location, as depicted in Figure 2.

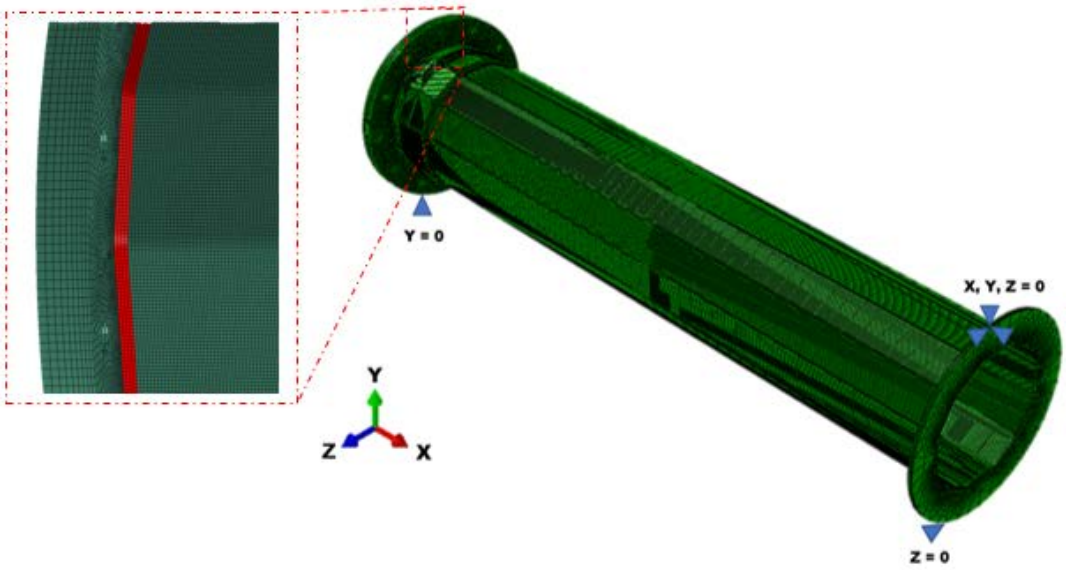

Figure 2. Mesh and boundary condition of the model.

4.2 Weld simulation Methodology

The welding simulation was performed using the Abaqus Welding Interface(AWI) plugin, developed by SIMULIA*(45)*. The AWI utility generates analysis steps for heat transfer and the static stress analysis. Based on sufficient user input, the plugin specifies the weld's surfaces and automatically creates weld chunks and passes, avoiding users' need to do this manually. A full description of the analysis methodology and numerical steps used in the AWI modeling routine can be found in the AWI Users' Manual *(49)*.

In AWI, the user specifies the weld and base material, heat transfer properties, and welding speed. A prescribed temperature approach is utilized by the AWI to represent the heat input from the weld torch. The deposition of the weld beads is in finite element sets called weld chunks. These are activated through a feature called "model change" along the specified weld path. This technique simulates filler metal's addition with the moving heat source by deactivating and activating the present weld chunk to ensure that each weld is introduced strain-free, known as the birth and death technique *(29)*. A prescribed temperature *(50)* of 1300°C is assigned as a boundary condition at the interface between the current weld bead chunks and the base material or already-deposited weld bead chunks.

The time duration required for the torch to pass the corresponding chunk of 15mm is set to 2.25 seconds as the temperature boundary condition. Temperature is linearly ramped for 10% percent of total time to the targeted prescribed temperature and held for the rest *(50)* using the ramping option.

The heat convective coefficient in air was hair = 10 W/m2/K *(44), (51)*. The effective emissivity was $\varepsilon = 0.9$, and the Stefan-Boltzmann constant was $\sigma = 5.67E\text{-}08$. The room temperature was specified to be 20°C. The HMIP was allowed to cool down for 3600s before the start of the

galvanizing process. The weld deposition sequence is illustrated in Figure 3, in which welding was carried out in the counterclockwise direction along the perimeter of the pole.

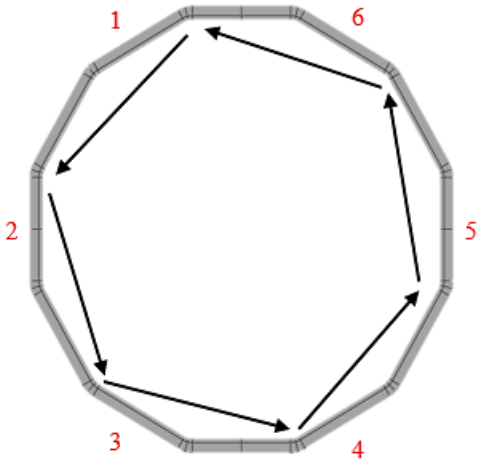

Figure 3. Weld Deposition Sequence.

4.3 Galvanizing simulation methodology

A coupled thermal-mechanical analysis was used to simulate the galvanization after the last step of the welding mechanical simulation. The resulting strain and stress fields from the welding process will be introduced as initial fields to the galvanizing process, capturing the cumulative effects from welding and galvanizing within the same model. Figure 4 illustrates the different finite element analysis that are conducted to model the sequence of welding and galvanizing. Details regarding the galvanizing simulation are provided in *(8)*. The Abaqus user Film subroutine was initiated to simulate the molten bath temperature of 445°C and a 1500 (W/m2K) heat convection coefficient. Conditional statements in the subroutine discerned used a reference plane the molted bath from the atmospheric temperature of 18°C and a heat convection coefficient of 1000 (W/m^2K). The dipping angle was taken as 8 degrees, and displacement boundary conditions enabled the different steps, i.e., dip, dwell, extract, and cool down steps. An illustration of the whole simulation procedure is provided in Figure 5.

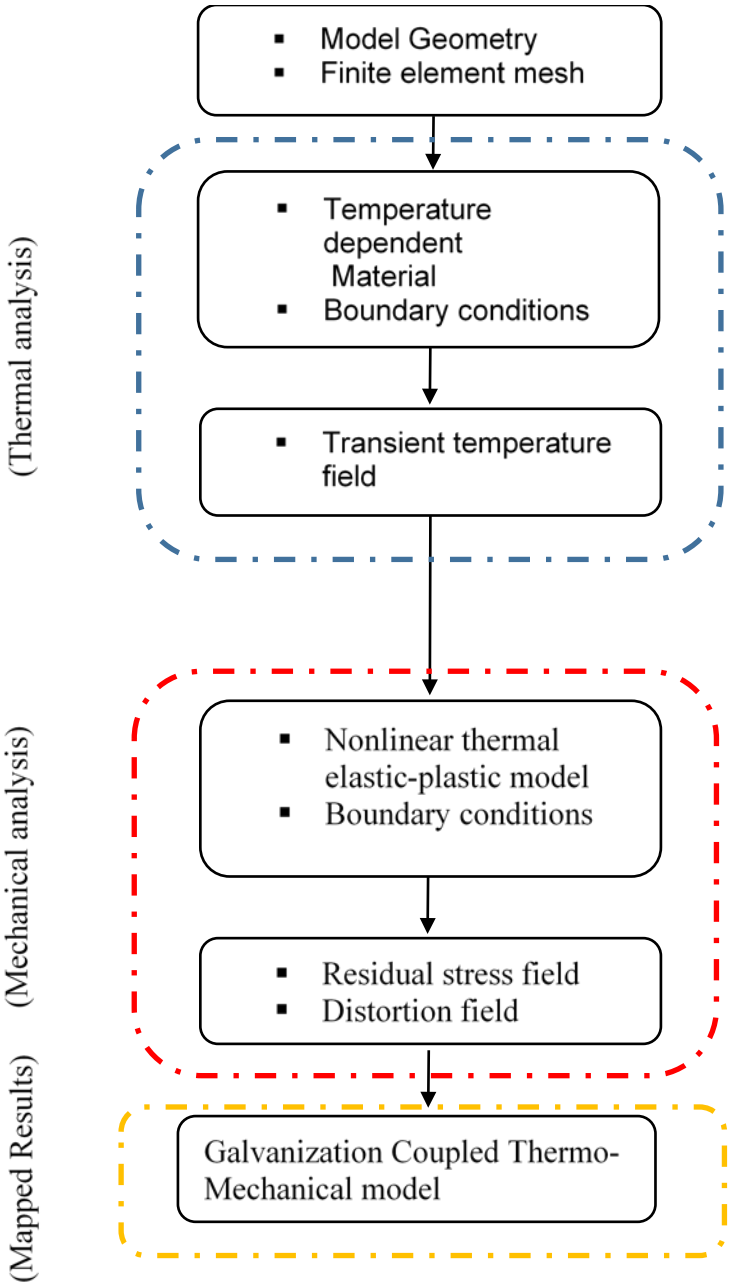

Figure 4. Cumulative Simulation Sequence.

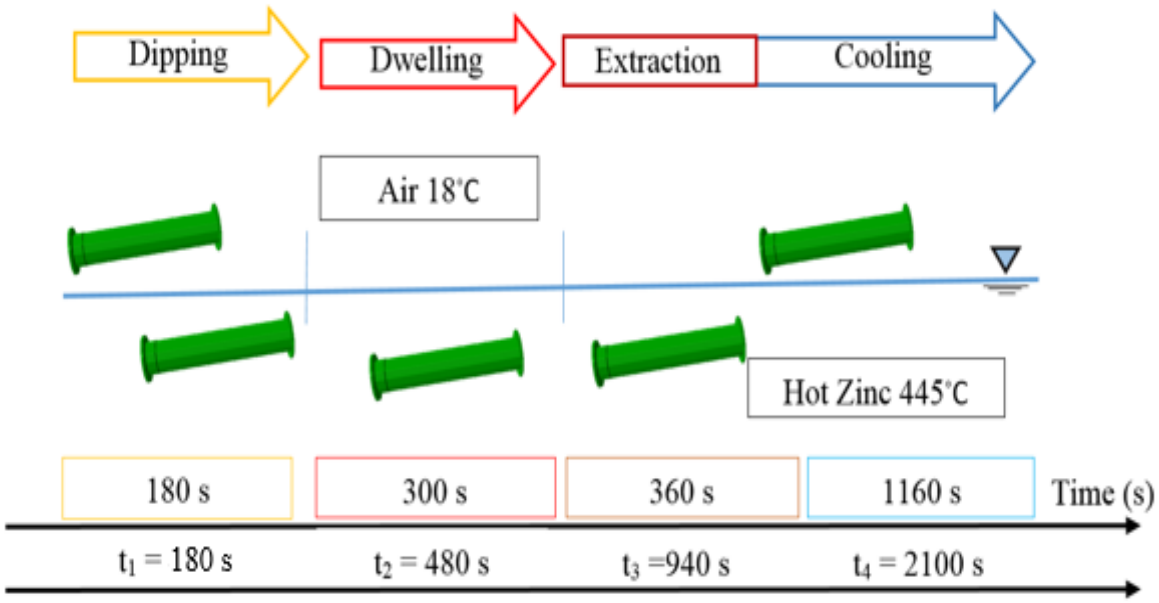

Figure 5. Simulation sequence: welding followed by galvanizing.

5. RESULTS

5.1. Welding-only analysis

Figure 6 shows the sequence of the welding process and how the torch advances through the welding path. It can be observed that temperature distribution ranges between 1500°C and room temperature; thus, this process has the potential of generating large residual stresses. The connection increase in temperature quickly and then the heat spreads through the HMIP's base. Both yielding and plastic deformation are known to be conducive to crack initiation, so the Von Mises stress and the equivalent plastic strain were explored as potential mechanical response variables indicative of crack initiation potential. Mises is a scalar value of stress computed to determine if a material yields or fracture. The equivalent plastic strain is cumulative over time; hence, it provides a history of the material's damage. Figure 7 shows that as the torch heats the elements along its path, it increases the Mises stress magnitude of those elements. Then, as the torch advances, the segments behind gradually cool down and decrease in stress magnitude. Figure 7 also illustrates the deformed shape of the pole during welding. It can be observed that the heated sections expand along the horizontal direction, creating an oval-like cross-section. Then, the pole gradually returns to its original shape.

To better study the stresses remaining on the pole's inner and outer surfaces at the end of the simulation (after the torch is removed), the stresses were extracted at a circumferential path located 18 mm away from the base (see Figure 8). Figure 9 shows the Mises stress at the inner and outer surface. There are twelve spikes in the plot; each spike occurs at a bend of the pole. The stresses obtained during welding were compared against the yield stress at room temperature. The stress spikes at the inner surface exceed the yield stress at room temperature, while the outer surface stresses are of lower magnitude, except for one of the spikes closes to the end of the path. However, note that the yield stress is lower at high temperatures. Thus, it is very likely that the yield stress was exceeded at almost every location along the circumferential path.

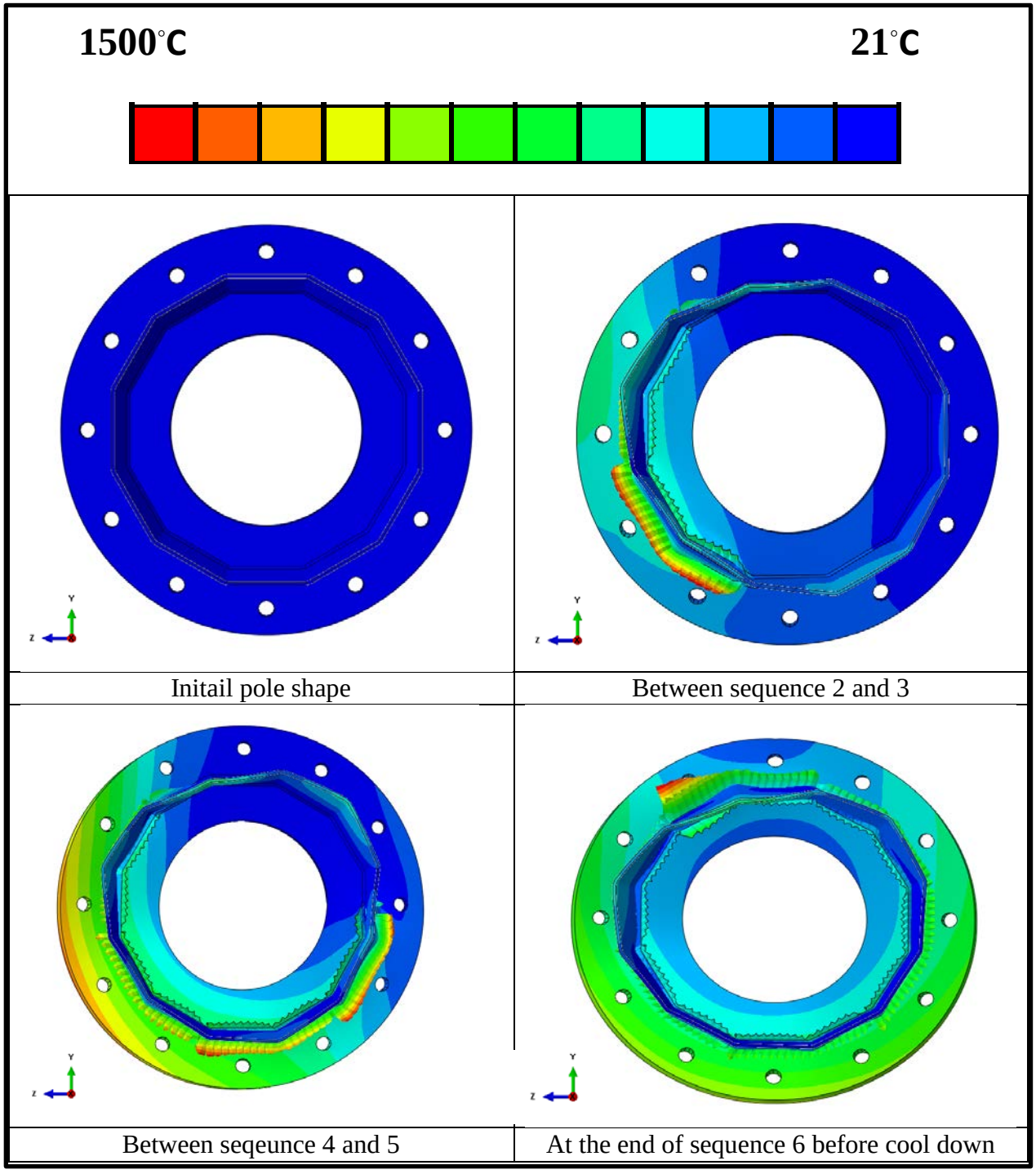

Figure 6. Temperature distribution during welding sequence.

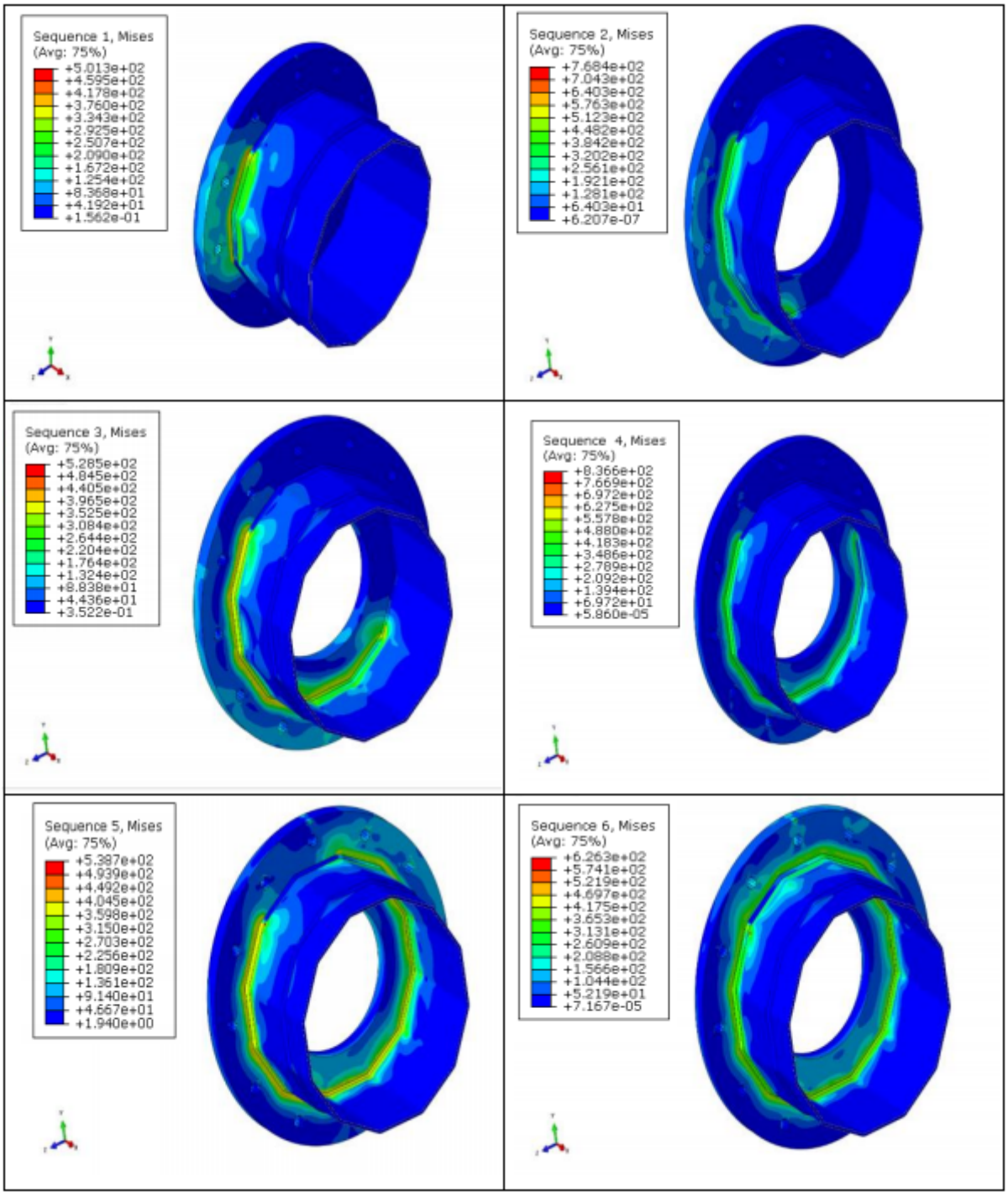
Sequence 1, Mises
(Avg: 75%)
+5.013e+02
+4.595e+02
+4.178e+02
+3.760e+02
+3.343e+02
+2.925e+02
+2.507e+02
+2.090e+02
+1.672e+02
+1.254e+02
+8.368e+01
+4.192e+01
+1.562e-01
Sequence 2, Mises
(Avg: 75%)
+7.684e+02
+7.043e+02
+6.403e+02
+5.763e+02
+5.123e+02
+4.482e+02
+3.842e+02
+3.202e+02
+2.561e+02
+1.921e+02
+1.281e+02
+6.403e+01
+6.207e-07
Sequence 3, Mises
(Avg: 75%)
+5.285e+02
+4.845e+02
+4.405e+02
+3.965e+02
+3.525e+02
+3.084e+02
+2.644e+02
+2.204e+02
+1.764e+02
+1.324e+02
+8.838e+01
+4.436e+01
+3.522e-01
Sequence 4, Mises
(Avg: 75%)
+8.366e+02
+7.669e+02
+6.972e+02
+6.275e+02
+5.578e+02
+4.880e+02
+4.183e+02
+3.486e+02
+2.789e+02
+2.092e+02
+1.394e+02
+6.972e+01
+5.860e-05
Sequence 5, Mises
(Avg: 75%)
+5.387e+02
+4.939e+02
+4.492e+02
+4.045e+02
+3.598e+02
+3.150e+02
+2.703e+02
+2.256e+02
+1.809e+02
+1.361e+02
+9.140e+01
+4.667e+01
+1.940e+00
Sequence 6, Mises
(Avg: 75%)
+6.263e+02
+5.741e+02
+5.219e+02
+4.697e+02
+4.175e+02
+3.653e+02
+3.131e+02
+2.609e+02
+2.088e+02
+1.566e+02
+1.044e+02
+5.219e+01
+7.167e-05

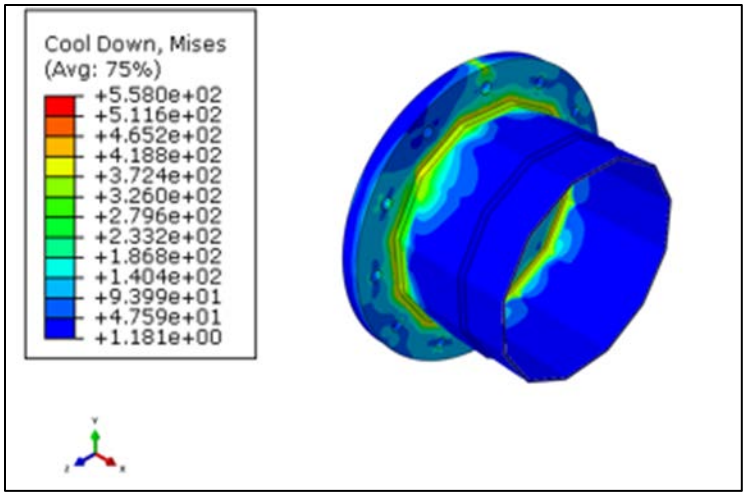

Figure 7. Mises stress and deformed shape during welding.

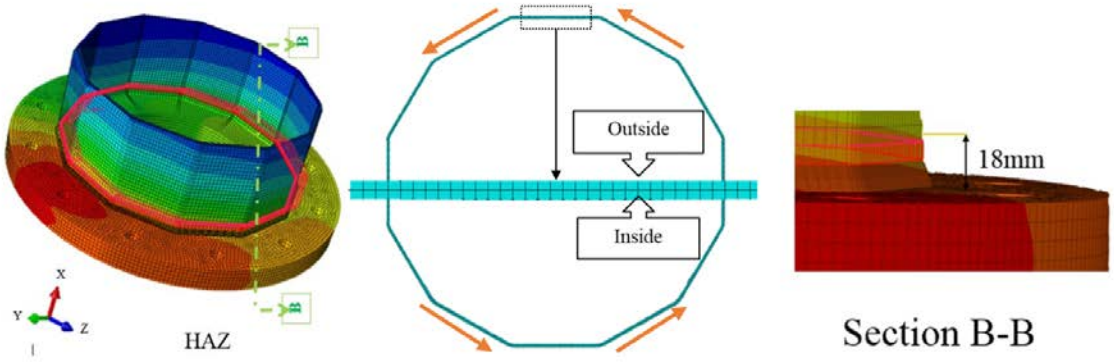

Figure 8. Path for extracting results.

The equivalent plastic strain (PEEQ) provides a clearer indication of the points along the path that underwent yielding, as this variable is a measure of unrecoverable deformation. In Figure 10, the inner surface shows PEEQ magnitudes higher than the outer surface magnitudes. The 11th bend (second bend from left to right) shows the highest spike (approaching 8000 microstrains at the inner surface and 5000 microstrains for the outer surface). This behavior is of interest as it would represent the weakest point on the pole. A hypothesis for this behavior is that this segment is the last to cool down; thus, it undergoes severe deformation to return to its original shape.

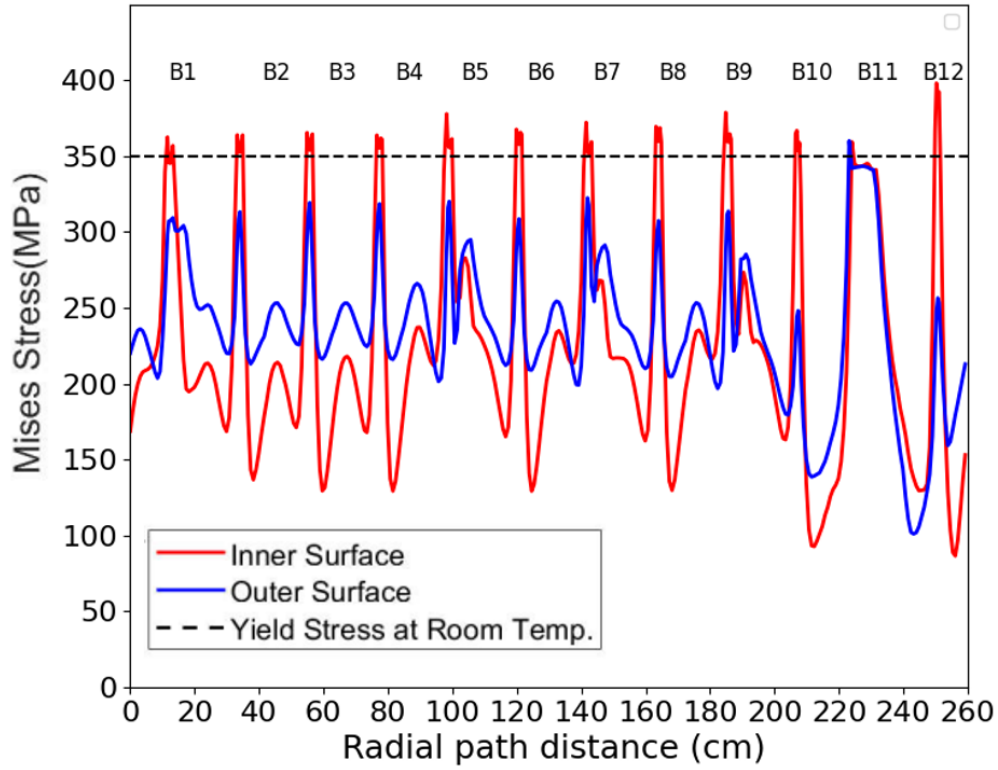

Figure 9. Mises stress at the end of the galvanization process.

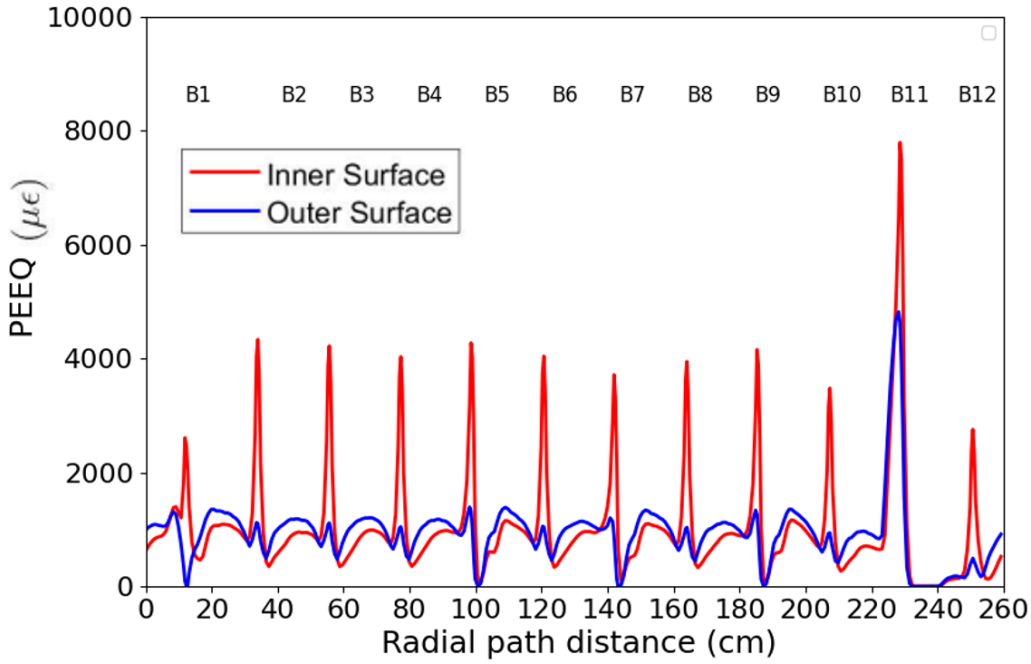

Figure 10. Equivalent plastic strain (PEEQ) at the end of the welding simulation.

5.2. Welding and Galvanizing analysis

Figure 11 illustrates the deformed shape during galvanizing, which accounts for the effects of the residual stresses generated during welding. It can be observed that the plate undergoes under bending deformation as it enters the molten zinc bath, while the pole stretches along the vertical direction, forming an oval-like shape. The pole and the base return to its original shape as the high mast illumination pole is extracted from the zinc bath and cools down.

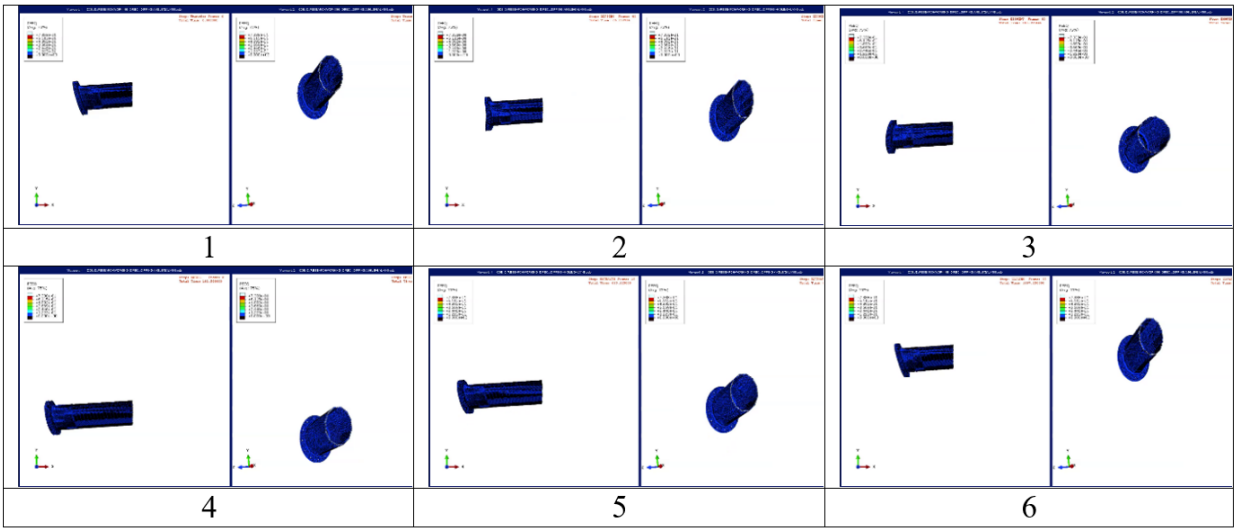

Figure 11. Deformation for post-galvanizing.

Figure 12 illustrates the cumulative residual stresses resulting from welding and galvanizing. It shows the Mises stress at the inner and outer surface for the same path shown in Figure 8. The results are compared against the maximum residual stresses resulting from a galvanizing only analysis performed by Nasouri et al. *(8)*. It can be observed that the stresses are higher when accounting for welding effects. Figure 13 performs the same comparison for the PEEQ. Although most sections along the path length have PEEQ values less than the maximum observed magnitude during a galvanizing only analysis, there is a spike that exceeds this value, reaching a magnitude of about 12,000 microstrains. This spike is the same as the one observed during welding.

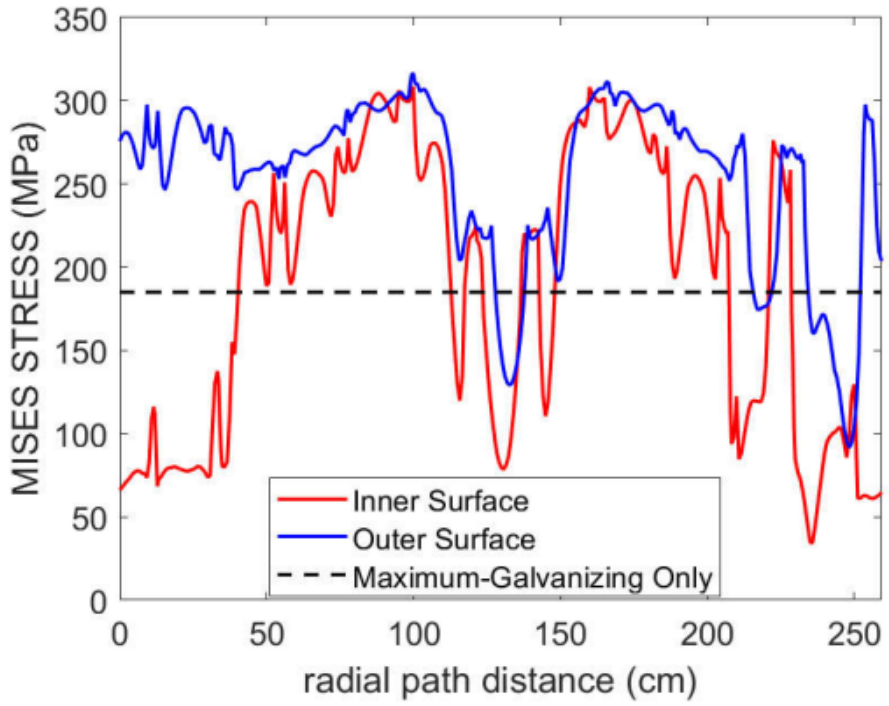

Figure 12. Mises stresses at the end of the galvanizing simulation.

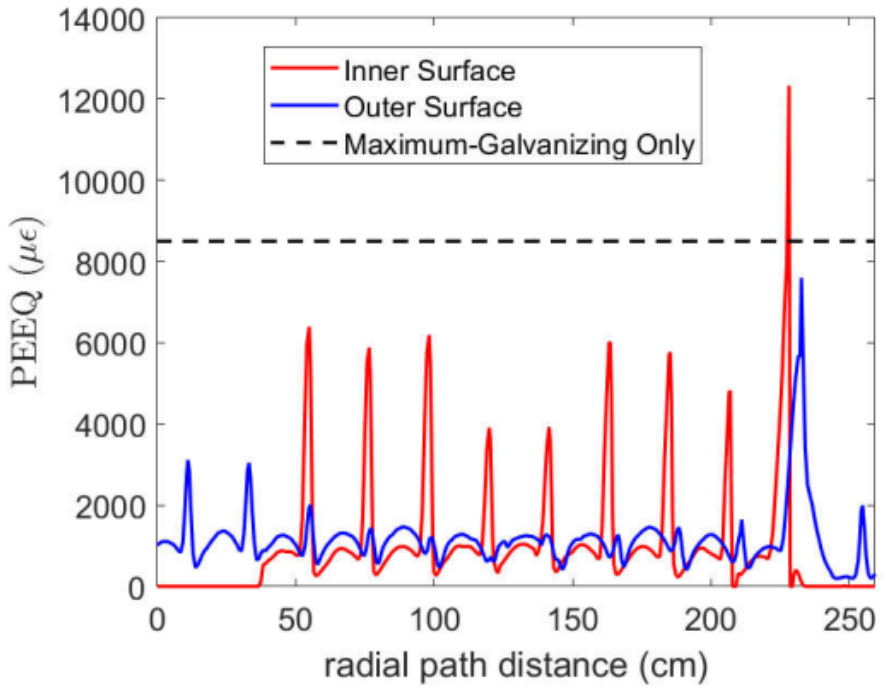

Figure 13. PEEQ at the end of the galvanizing simulation.

5.3. Parametric Study

The speed of submersion was adjusted in the simulation accounting for the cumulative effects of welding and galvanizing. It can be observed from Figure 14 and Figure 15 that as the speed increases, the stress magnitude and PEEQ decreases. The effect of speed is more notorious between 25 mm/s and 63 mm/s. The variation between 63 mm/s and 89 mm/s is less evident.

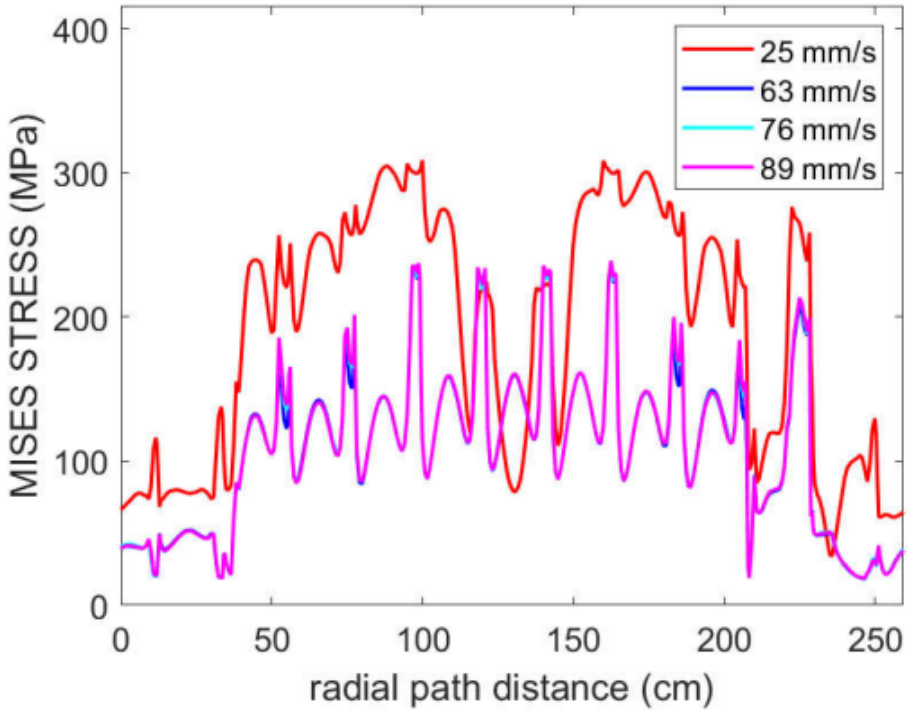

Figure 14. Variation in stresses as a function of speed.

Figure 16 and Figure 17 compare the maximum stresses at both the inner and outer surfaces for different speeds. In general, the Mises stress and PEEQ at the inner surface are larger at the inner surface than the outer surface of the path. The maximum values at the speeds between 63 mm/s and 89 mm/s seem to have reached a plateau, suggesting that after a certain speed the improvements with respect to speed are less apparent. These results agree with the observations highlighted by Nasouri et al. *(8)*, which concluded that submerging the HMIPs at faster speeds is favorable to reduce the residual stresses and PEEQs generated during the galvanizing process.

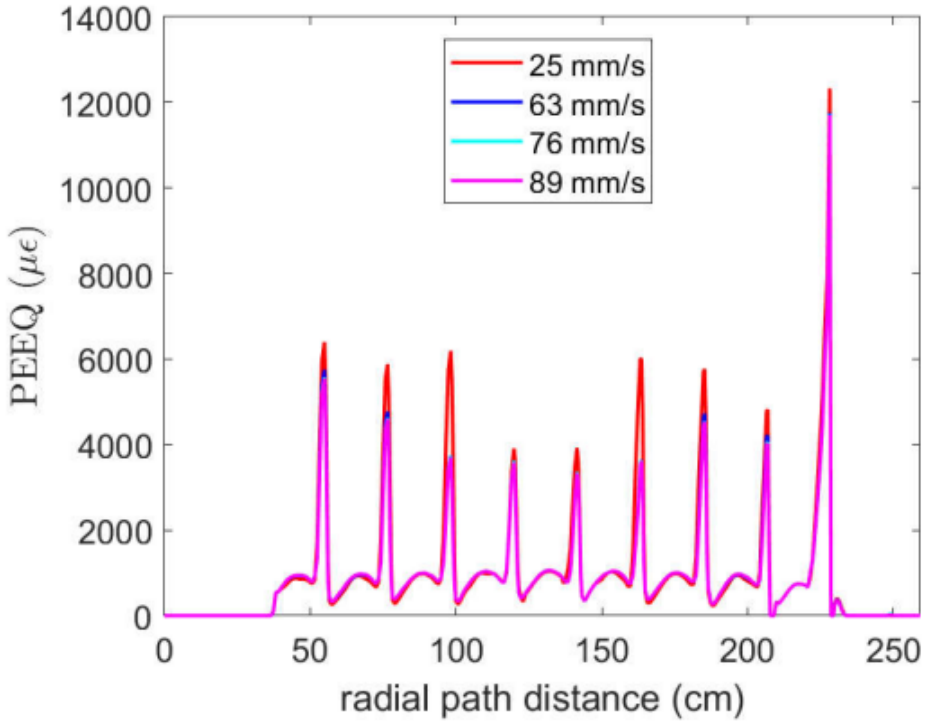

Figure 15. Variation in PEEQ as a function of speed.

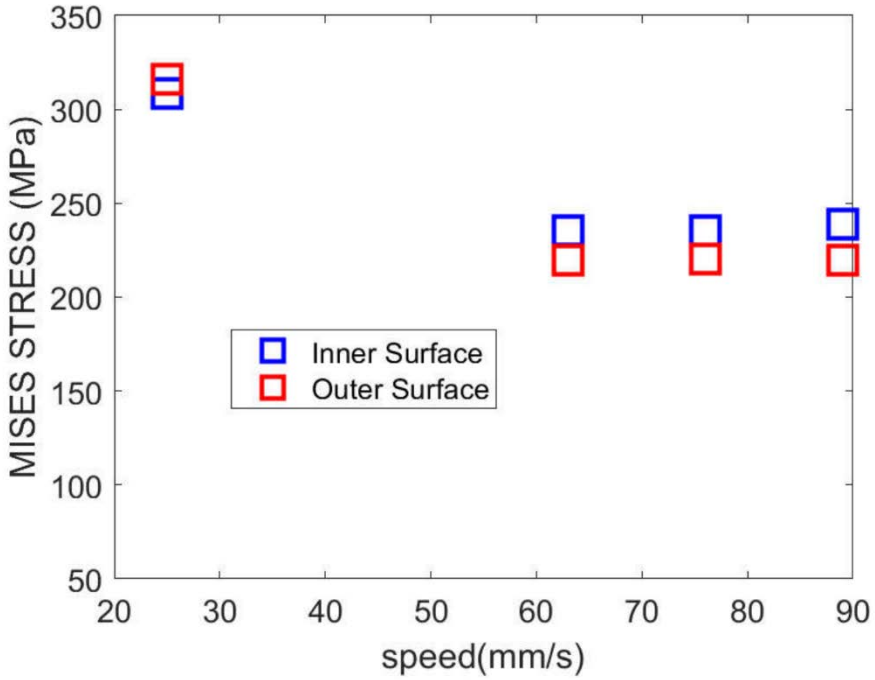

Figure 16. Maximum Mises stress as a function of speed.

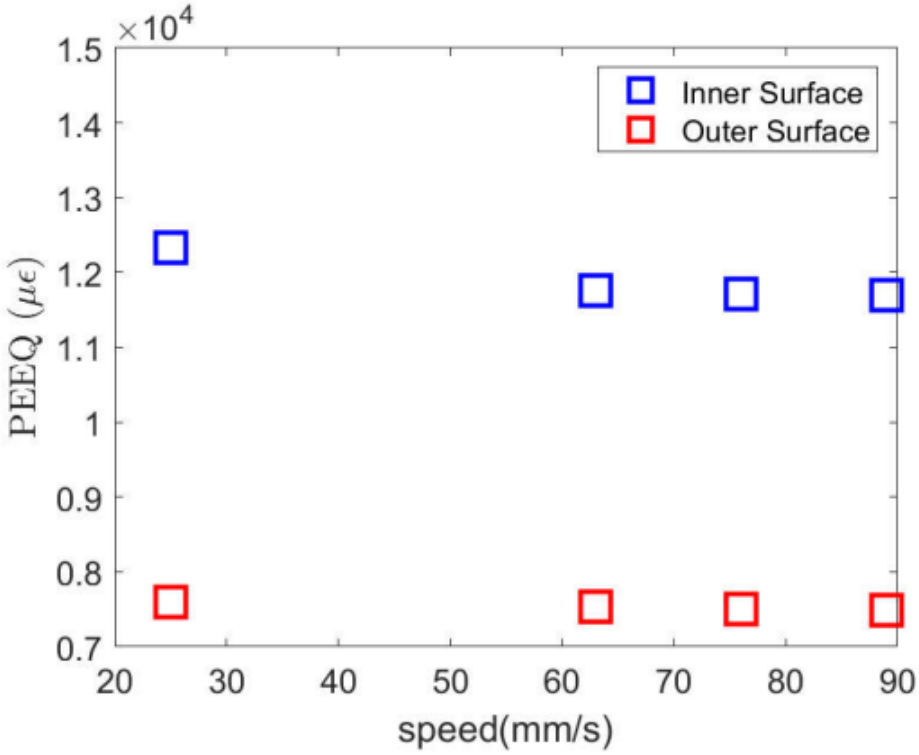

Figure 17. Maximum PEEQ as a function of speed.

The angle of speed was adjusted between zero and twelve degrees, as shown in Figure 18 and Figure 19. The stress values provided very similar results for all the considered cases. The PEEQ values seem to be higher for the angle submerged at eight degrees. Figure 20 confirms that the stress values seem to be independent of the angle of submersion. Figure 21 shows that the inner surface maximum PEEQ seems to be higher at intermediate values (4 and 8 degrees). On the other hand, the maximum PEEQ at the outer surface, seems to be invariant for angles smaller than 10 degrees, but it peaks off at 12 degrees. These observations do not provide a clear trend as the one reported by Nasouri et al. *(8)* from a galvanizing only analysis, who recommended to submerge the pole at larger angles as the stresses and PEEQ decreased in magnitude with larger angles.

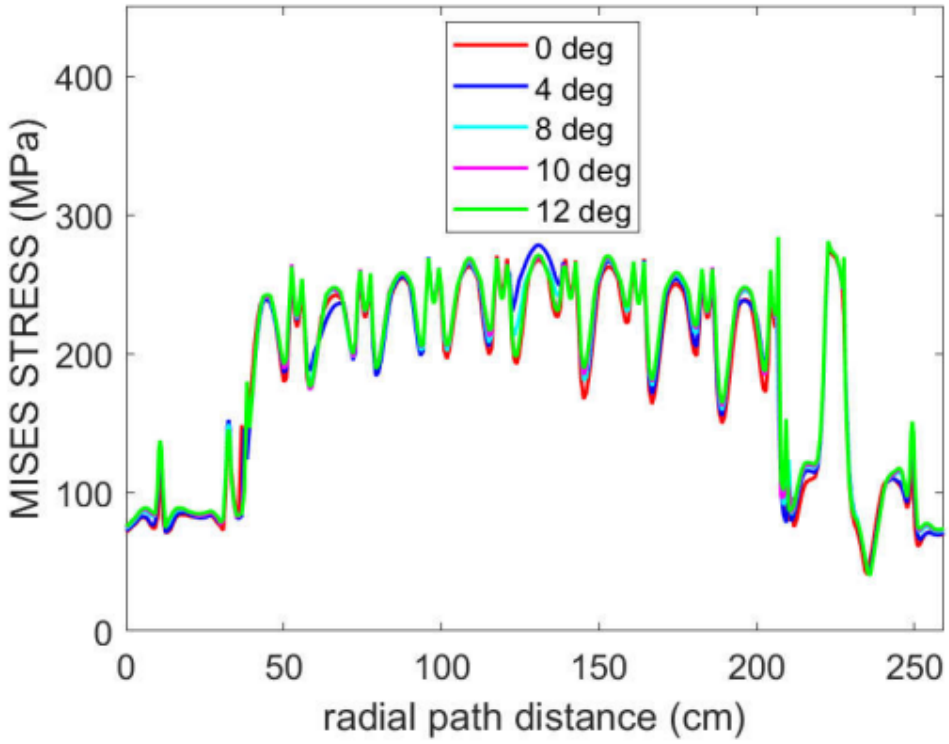

Figure 18. Stresses as a function of angle of inclination.

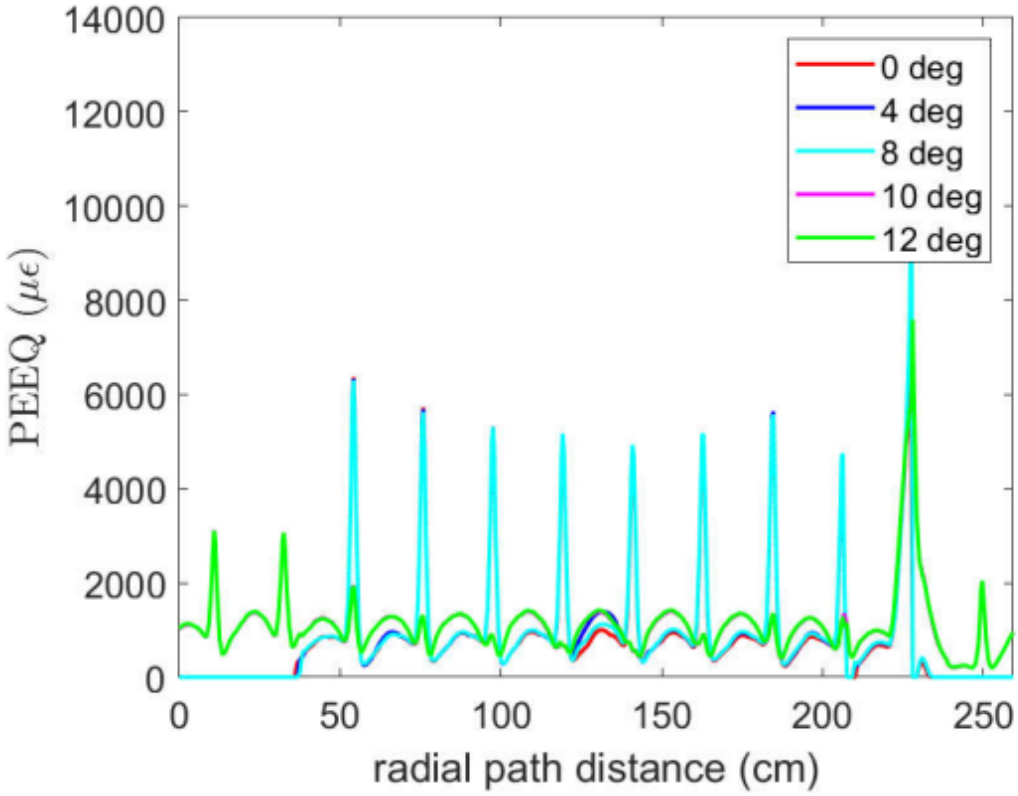

Figure 19. PEEQ as a function of angle of inclination.

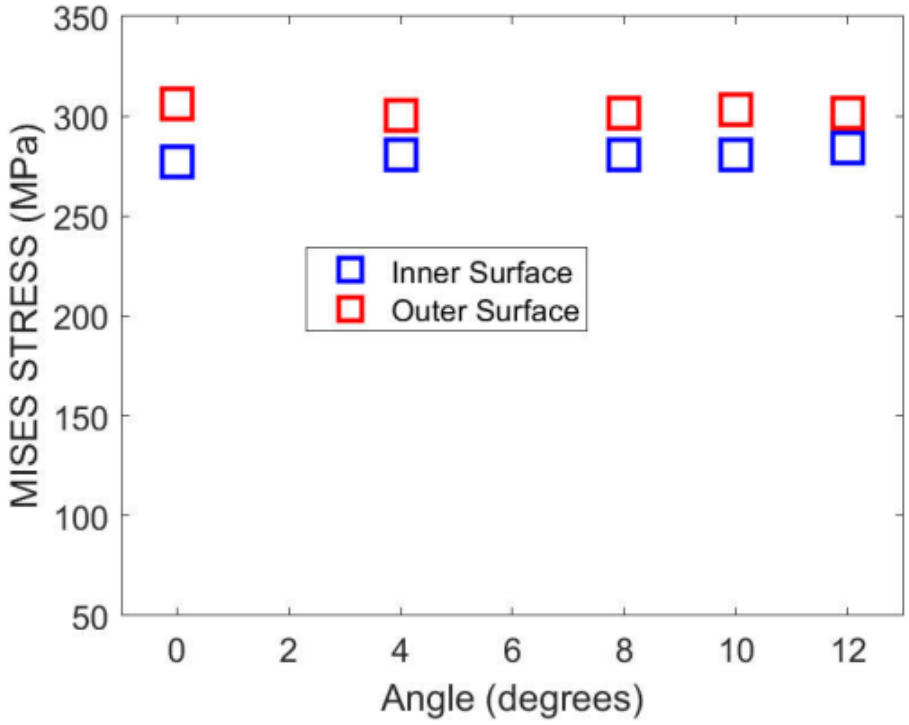

Figure 20. Maximum stress as a function of angle of inclination.

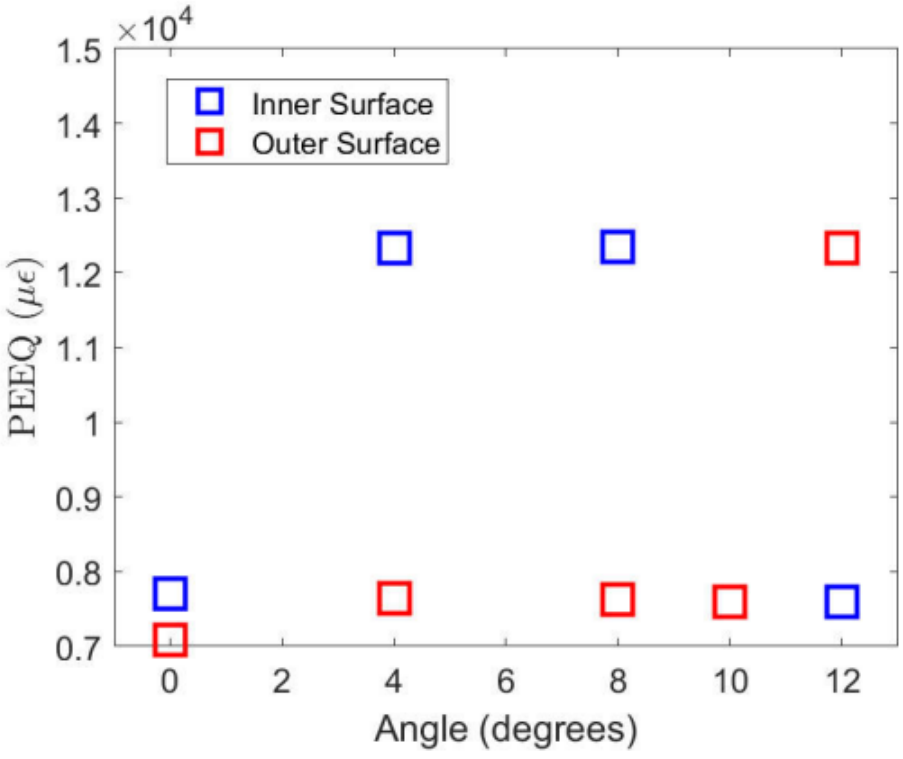

Figure 21. Maximum PEEQ as a function of angle of inclination.

Also, the welding results were repeated for different torch values, as observed in Figure 22 and Figure 23. It was observed that the stresses increase with the torch magnitude as expected. Also, a large peak in PEEQ was observed for different temperature magnitudes at segment S-12. The magnitude of the spike was shown to increase with larger torch temperature magnitudes. Other variations that could be considered in the welding analysis includes preheating. Preheating is known to minimize the temperature differential between the welding arc and base material and slow the down the cooling rate. These effects may contribute to lowering the magnitudes of PEEQ and Mises stress on the HMIP. Consequently, preheating may reduce the probability of weld-toe cracks and large PEEQ spikes as shown in Figure 23.

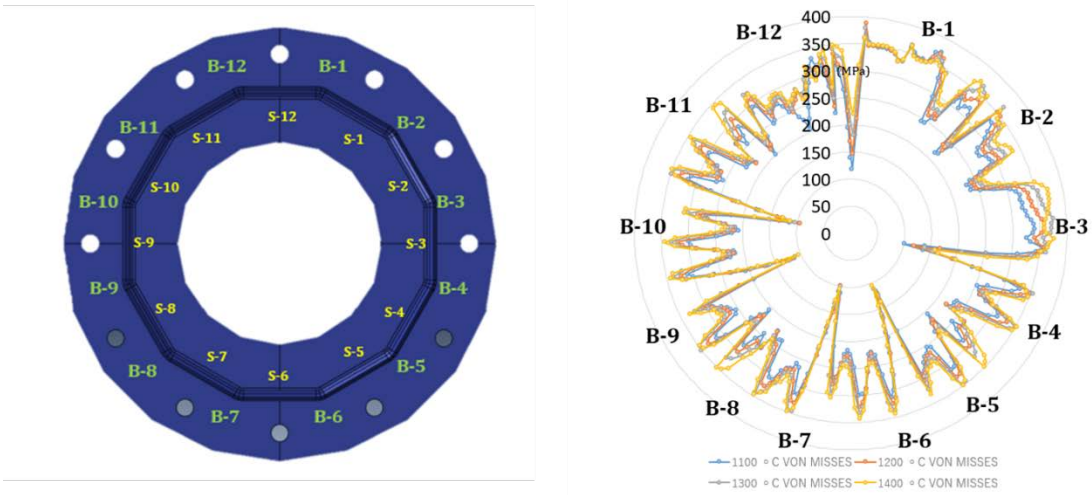

Figure 22. Mises stress as a function of torch temperature.

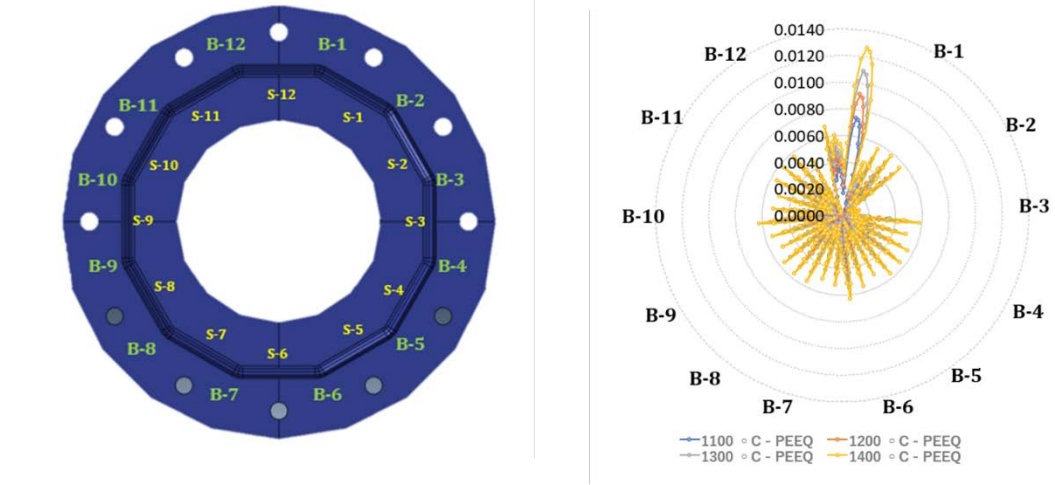

Figure 23. PEEQ as a function of torch temperature.

6. CONCLUSIONS

Cracks at the pole-to-base plate connection of High Mast Illumination Poles (HMIPs) constitute a significant source of concern to highway transportation officials. These cracks are typically identified post-galvanizing and result from the thermally-induced deformations induced during the galvanizing process. However, each of the fabricating stages involved in the manufacturing of HMIPs, i.e., cold working, welding, and hot-dip galvanizing, induce residual stresses in steel. Thus, these cracks cannot be merely credited to the galvanizing process.

In this study, finite element modeling was used to analyze the response of the HMIPs under thermomechanical loading conditions. A reliable high-resolution finite element (FE) model capable of simulating the thermo-mechanical response of HMIPs throughout its manufacturing process, both welding and galvanizing, including dipping, dwelling, extraction, and cooling, was developed. This model is based on the TxDOT pole-to-base plate connection detail. Welding was modeled using the plug-in Abaqus Welding Interface (AWI). First, a heat transfer analysis is performed to generate a temperature history based on a prescribed temperature (called the torch temperature) applied at the weld location. The thermal analysis is automatically followed by a mechanical analysis that captures the welding process's elastic and inelastic effects. Then, the welding stress results were used as initial input to the galvanizing analysis. The cumulative stress results were compared against simulations that only considered the galvanizing process. A parametric study was then conducted to quantify the variation in the residual stresses and PEEQ resulting after the galvanizing of HMIPs. The control variables of the study were speed, angle of inclination, and torch magnitude.

The results revealed that the cumulative effects of the different processes involved in the manufacturing of HMIPs contribute to the formation of galvanizing cracks in HMIPs. Also, increasing the dipping submersion speed during galvanizing and lowering the torch temperature magnitude during welding results in fewer zones prone to cracking. Altering the angle of inclination effect did not have a significant impact on the results. Performing variations in the manufacturing practices used to fabricate HMIPs can reduce the extensive inspection procedures conducted post-galvanizing to identify cracks.

Future simulations performed with the approach developed in this study will serve to identify geometric configurations that make HMIPs less vulnerable to damage during their manufacturing, evaluate the likelihood of crack for the types of connections details used by the different state department of Transportations, and propose modifications to the welding and galvanizing procedures to minimize the residual stresses induced during these processes.

REFERENCES

1. T. H. Anderson, "Fatigue Life Investigation of Traffic Signal Mast-Arm Connection Details," p. 137.
2. N. Suksawang, B. Mintz, and A. Mirmiran, "Remedial action for failed pole/base plate weld on high mast lighting pole (HMLP) : final report, December 2009.," Dec. 2009, [Online]. Available: https://rosap.ntl.bts.gov/view/dot/17491.
3. "(3) Sensitivity of Predicted Temperature in a Fillet Weld T-Joint to Parameters Used in Welding Simulation with Prescribed Temperature Approach | Request PDF," *ResearchGate*. https://www.researchgate.net/publication/324528884_Sensitivity_of_Predicted_Temperature_in_a_Fillet_Weld_T-Joint_to_Parameters_Used_in_Welding_Simulation_with_Prescribed_Temperature_Approach (accessed Jul. 08, 2020).
4. K. Nguyen, R. Nasouri, C. R. Bennett, A. Matamoros, J. Li, and A. H. Montoya, "Thermomechanical Modeling of Welding and Galvanizing a Steel Beam Connection Detail to Examine Susceptibility to Cracking," *Mater. Perform. Charact.*, vol. 7, no. 2, p. 20170115, Feb. 2018, doi: 10.1520/MPC20170115.
5. R. J. Connor, S. H. Collicott, A. M. DeSchepper, R. J. Sherman, and J. A. Ocampo, "Fatigue Loading and Design Methodology for High-Mast Lighting Towers," *NCHRP Rep.*, no. 718, Art. no. Project 10-74, 2012, Accessed: Jul. 08, 2020. [Online]. Available: https://trid.trb.org/view/1138812.
6. M. Dawood, R. Goyal, H. Dhonde, and T. Bradberry, "Fatigue Life Assessment of Cracked High-Mast Illumination Poles," *J. Perform. Constr. Facil.*, vol. 28, no. 2, pp. 311–320, Apr. 2014, doi: 10.1061/(ASCE)CF.1943-5509.0000438.
7. J. R. Kleineck, "Galvanizing crack formation at base plate to shaft welds of high mast illumination poles," thesis, 2011.
8. R. Nasouri, K. Nguyen, A. Montoya, A. Matamoros, C. Bennett, and J. Li, "Simulating the hot dip galvanizing process of high mast illumination poles. Part I: Finite element model development," *J. Constr. Steel Res.*, vol. 162, p. 105705, Nov. 2019, doi: 10.1016/j.jcsr.2019.105705.
9. "ASTM: Standard practice for safeguarding against... - Google Scholar." https://scholar.google.com/scholar_lookup?title=Standard%20Practice%20for%20Safeguarding%20Against%20Embrittlement%20of%20Hot-Dip%20Galvanized%20Structural%20Steel%20Products%20and%20Procedure%20for%20Detecting%20Embrittlement&author=ASTM-A143&publication_year=2014 (accessed Jul. 10, 2020).
10. “ASTM: 123: Standard Specification for Zinc (Hot-Dip... - Google Scholar.” https://scholar.google.com/scholar_lookup?title=Standard%20Specification%20for%20Zinc%20(Hot-Dip%20Galvanized)%20Coatings%20on%20Iron%20and%20Steel%20Products.%20Pressed%20and%20Forged%20Steel%20Shapes%2C%20Plates%2C%20Bars%2C%20and%20Strip&author=ASTM-A123&publication_year=2017 (accessed Jul. 10, 2020).
11. M. Sun and Z. Ma, "Effects of heat-treatment and hot-dip galvanizing on mechanical properties of RHS," *J. Constr. Steel Res.*, vol. 153, pp. 603–617, Feb. 2019, doi: 10.1016/j.jcsr.2018.11.012.

12. M. Pourmajidian and J. R. McDermid, "On the reactive wetting of a medium-Mn advanced high-strength steel during continuous galvanizing," *Surf. Coat. Technol.*, vol. 357, pp. 418–426, Jan. 2019, doi: 10.1016/j.surfcoat.2018.10.028.
13. C. S. Pool, "Effect of galvanization on the fatigue strength of high mast illumination poles," thesis, 2010.
14. A. Stam, N. Richman, C. Pool, C. Rios, T. Anderson, and K. Frank, "Fatigue Life of Steel Base Plate to Pole Connections for Traffic Structures," p. 165.
15. K. Nguyen, R. Nasouri, C. Bennett, A. Matamoros, and J. Li, "DISTORTION OF STEEL PLATE GIRDERS DUE TO HOT-DIP GALVANIZING," p. 15.
16. T. J. Kinstler, "Current Knowledge of the Cracking of Steels During Galvanizing A Synthesis of the Available Technical Literature and Collective Experience for the American Institute of Steel Construction," 2005.
17. D. Radaj, C. M. Sonsino, and W. Fricke, *Fatigue Assessment of Welded Joints by Local Approaches*. Woodhead Publishing, 2006.
18. B. Chang, B. M. Phares, P. P. Sarkar, and T. J. Wipf, "Development of a Procedure for Fatigue Design of Slender Support Structures Subjected to Wind-Induced Vibration:," *Transp. Res. Rec.*, Jan. 2009, doi: 10.3141/2131-03.
19. "Dexter: Investigation of cracking of high-mast lighting... - Google Scholar." https://scholar.google.com/scholar_lookup?title=Investigation%20of%20Cracking%20of%20High-Mast%20Lighting%20Structures&author=R.%20Dexter&publication_year=2004 (accessed Jul. 11, 2020).
20. "Dijkstra: Fatigue strength of tubular T-and X-joints - Google Scholar." https://scholar.google.com/scholar_lookup?title=Fatigue%20strength%20of%20tubular%20T-and%20X-joints&author=O.D.%20Dijkstra&publication_year=1980 (accessed Jul. 11, 2020).
21. S. Roy, Y. C. Park, R. Sause, and J. W. Fisher, "Fatigue Resistance of Pole-to-Base Plate Connections in High Level Lighting Structures," pp. 170–181, Apr. 2012, doi: 10.1061/41130(369)17.
22. M. A. Morovat *et al.*, "Fatigue Resistance and Reliability of High Mast Illumination Poles (HMIPs) with Pre-Existing Cracks: Final Report," Art. no. FHWA/TX-18/0-6829-1, Nov. 2018, Accessed: Jul. 08, 2020. [Online]. Available: https://trid.trb.org/view/1573428.
23. M. K. Warpinski, "The effect of base connection geometry on the fatigue performance of welded socket connections in multisided highmast lighting towers," 2006.
24. J. M. Ocel, *The behavior of thin hollow structural section (HSS) to plate connections*. University of Minnesota, 2006.
25. A. P. Stam, "Fatigue Performance of Base Plate Connections Used in High Mast Lighting Towers," PhD Thesis, University of Texas at Austin, 2009.
26. Z. Chen, Y. Xiong, H. Qiu, G. Lin, and Z. Li, "Stress intensity factor-based prediction of solidification crack growth during welding of high strength steel," *J. Mater. Process. Technol.*, vol. 252, pp. 270–278, Feb. 2018, doi: 10.1016/j.jmatprotec.2017.09.031.
27. S. H. Oh *et al.*, "Evaluation of J-groove weld residual stress and crack growth rate of PWSCC in reactor pressure vessel closure head," *J. Mech. Sci. Technol.*, vol. 29, no. 3, pp. 1225–1230, Mar. 2015, doi: 10.1007/s12206-015-0236-5.
28. H. Takazawa and N. Yanagida, "Effect of creep constitutive equation on simulated stress mitigation behavior of alloy steel pipe during post-weld heat treatment," *Int. J. Press. Vessels Pip.*, vol. 117–118, pp. 42–48, May 2014, doi: 10.1016/j.ijpvp.2013.10.008.

29. K. Seleš, M. Perić, and Z. Tonković, "Numerical simulation of a welding process using a prescribed temperature approach," *J. Constr. Steel Res.*, vol. 145, pp. 49–57, Jun. 2018, doi: 10.1016/j.jcsr.2018.02.012.
30. C. Heinze, C. Schwenk, and M. Rethmeier, "Effect of heat source configuration on the result quality of numerical calculation of welding-induced distortion," *Simul. Model. Pract. Theory*, vol. 20, no. 1, pp. 112–123, Jan. 2012, doi: 10.1016/j.simpat.2011.09.004.
31. X. K. Zhu and Y. J. Chao, "Effects of temperature-dependent material properties on welding simulation," *Comput. Struct.*, vol. 80, no. 11, pp. 967–976, May 2002, doi: 10.1016/S0045-7949(02)00040-8.
32. G. H. Little and A. G. Kamtekar, "The effect of thermal properties and weld efficiency on transient temperatures during welding," *Comput. Struct.*, vol. 68, no. 1, pp. 157–165, Jul. 1998, doi: 10.1016/S0045-7949(98)00040-6.
33. E. Armentani, R. Esposito, and R. Sepe, "The effect of thermal properties and weld efficiency on residual stresses in welding," *J. Achiev. Mater. Manuf. Eng.*, vol. 20, p. 4, 2007.
34. A. A. Bhatti, Z. Barsoum, H. Murakawa, and I. Barsoum, "Influence of thermo-mechanical material properties of different steel grades on welding residual stresses and angular distortion," *Mater. Des. 1980-2015*, vol. 65, pp. 878–889, Jan. 2015, doi: 10.1016/j.matdes.2014.10.019.
35. M. Feldmann, T. Pinger, D. Schäfer, R. Pope, W. Smith, and G. Sedlacek, "Hot-dip-zinc-coating of prefabricated structural steel components," *JRC Sci. Tech. Rep.*, 2010.
36. "ABAQUS/CAE User's Manual (v6.6)." https://classes.engineering.wustl.edu/2009/spring/mase5513/abaqus/docs/v6.6/books/usi/default.htm (accessed Jul. 10, 2020).
37. "Sudnik: Validation of computerised simulation of... - Google Scholar." https://scholar.google.com/scholar_lookup?title=Validation%20of%20computerised%20simulation%20of%20welding%20processes&publication_year=1997&author=W.%20Sudnik&author=D.%20Radaj&author=W.%20Erofeew (accessed Jul. 12, 2020).
38. L.-E. Lindgren, "Numerical modelling of welding," *Comput. Methods Appl. Mech. Eng.*, vol. 195, no. 48, pp. 6710–6736, Oct. 2006, doi: 10.1016/j.cma.2005.08.018.
39. L.-E. Lindgren, "Finite Element Modeling and Simulation of Welding Part 1: Increased Complexity," *J. Therm. Stress.*, vol. 24, no. 2, pp. 141–192, Feb. 2001, doi: 10.1080/01495730150500442.
40. L.-E. Lindgren, "Finite Element Modeling and Simulation of Welding. Part 3: Efficiency and Integration," *J. Therm. Stress.*, vol. 24, no. 4, pp. 305–334, Apr. 2001, doi: 10.1080/01495730151078117.
41. "Radaj: Welding residual stresses and distortion - Google Scholar." https://scholar.google.com/scholar_lookup?title=Welding%20Residual%20Stresses%20and%20Distortion%20Calculation%20and%20measurement&publication_year=2003&author=D.%20Radaj (accessed Jul. 12, 2020).
42. W. L. Oberkampf and T. G. Trucano, "Verification and validation in computational fluid dynamics," *Prog. Aerosp. Sci.*, vol. 38, no. 3, pp. 209–272, Apr. 2002, doi: 10.1016/S0376-0421(02)00005-2.
43. A. Pilipenko, "Computer simulation of residual stress and distortion of thick plates in multi-electrode submerged arc welding. Their mitigation techniques," no. 1289, p. 228.

44. M. Perić *et al.*, "Numerical analysis and experimental investigation of welding residual stresses and distortions in a T-joint fillet weld," *Mater. Des.*, vol. 53, pp. 1052–1063, Jan. 2014, doi: 10.1016/j.matdes.2013.08.011.
45. D. S. Simulia, "Abaqus 2017." 2017.
46. K.-H. Chang and C.-H. Lee, "Finite element analysis of the residual stresses in T-joint fillet welds made of similar and dissimilar steels," *Int. J. Adv. Manuf. Technol.*, vol. 41, no. 3, p. 250, Apr. 2008, doi: 10.1007/s00170-008-1487-4.
47. T.-L. Teng, C.-P. Fung, P.-H. Chang, and W.-C. Yang, "Analysis of residual stresses and distortions in T-joint fillet welds," *Int. J. Press. Vessels Pip.*, vol. 78, no. 8, pp. 523–538, Aug. 2001, doi: 10.1016/S0308-0161(01)00074-6.
48. M. Siddique, M. Abid, H. F. Junejo, and R. A. Mufti, "3-D Finite Element Simulation of Welding Residual Stresses in Pipe-Flange Joints: Effect of Welding Parameters," *Mater. Sci. Forum*, vol. 490–491, pp. 79–84, Jul. 2005, doi: 10.4028/www.scientific.net/MSF.490-491.79.
49. Simulia, "Abaqus Welding Interface (AWI)—User's Manual." 2017.
50. "FINITE ELEMENT MODELING AND SIMULATION OF WELDING PART 1: INCREASED COMPLEXITY: Journal of Thermal Stresses: Vol 24, No 2." https://www.tandfonline.com/doi/abs/10.1080/01495730150500442 (accessed Jul. 10, 2020).
51. A. M. Malik, E. M. Qureshi, N. Ullah Dar, and I. Khan, "Analysis of circumferentially arc welded thin-walled cylinders to investigate the residual stress fields," *Thin-Walled Struct.*, vol. 46, no. 12, pp. 1391–1401, Dec. 2008, doi: 10.1016/j.tws.2008.03.011.